HHS Public Access

Author manuscript

*Transplantation*. Author manuscript; available in PMC 2017 June 01.

Published in final edited form as:

*Transplantation*. 2016 June ; 100(6): 1198–1210. doi:10.1097/TP.0000000000001137.

# Nox2 and Cyclosporine-Induced Renal Hypoxia

**Arjang Djamali, MD**[1], **Nancy A Wilson, PhD**[1], **Elizabeth A Sadowski, MD**[2], **Wei Zha, PhD**[3], **David Niles**[3], **Omeed Hafez**[1], **Justin R Dorn**[1], **Tom R Mehner**[1], **Paul C. Grimm, MD**[4], **F. Michael Hoffmann, PhD**[5], **Weixiong Zhong, MD, PhD**[6], **Sean B Fain, PhD**[3], and **Shannon R. Reese, MS**[1]

[1]University of Wisconsin Department of Medicine | Division of Nephrology, Madison, WI

[2]University of Wisconsin Department of Radiology | Madison, WI

[3]University of Wisconsin Department of Medical Physics | Madison, WI

[4]Stanford University | Division of Pediatric Nephrology, San Francisco, CA

[5]University of Wisconsin Cancer Center | McArdle Institute, Madison, WI

[6]University of Wisconsin Department of Pathology and Laboratory Medicine

## Abstract

**Background—**We hypothesized that Nox2 plays an important role in cyclosporine A (CsA)-induced chronic hypoxia.

Corresponding Author: Arjang Djamali, MD, 5142 MFCB, 1685 Highland Avenue, Madison, WI, ; Email: axd@medicine.wisc.edu.
Authors

| | Design | Data Collection | Analyses | Manuscript Editing |
|---|---|---|---|---|
| Arjang Djamali | X | | X | X |
| Nancy Wilson | X | | X | X |
| Elizabeth Sadowski | X | | X | X |
| Wei Zha | | X | X | X |
| David Niles | | X | X | X |
| Omeed Hafez | | X | X | X |
| Justin Dorn | | X | X | X |
| Tom Mehner | | X | X | X |
| Paul Grimm | X | | X | X |
| Michael Hoffmann | X | | X | X |
| Weixiong Zhong | X | | X | X |
| Sean Fain | X | | X | X |
| Shannon Reese | X | | X | X |

Conflicts. The authors declare no conflicts of interest.

**Methods—**We tested this hypothesis in Fisher 344 rats, C57BL/6J wild type and Nox2−/− mice, and in liver transplant recipients with chronic CsA nephrotoxicity. We used noninvasive molecular imaging (BOLD and DCE MRI) and molecular diagnostic tools to assess intrarenal oxygenation and perfusion, and the molecular phenotype of CsA nephrotoxicity.

**Results—**We observed that chemical and genetic inhibition of Nox2 in rats and mice resulted in the prevention of CsA-induced hypoxia independent of regional perfusion (BOLD and DCE MRI, pimonidazole, HIF1-α). Nox2 knockout was also associated with decreased oxidative stress (Nox2, HIF-1α, hydrogen peroxide, HNE), and fibrogenesis (α-SMA, picrosirius red, trichrome, vimentin). The molecular signature of chronic CsA nephrotoxicity using transcriptomic analyses demonstrated significant changes in 40 genes involved in injury-repair, metabolism, and oxidative stress in Nox2−/− mice. Immunohistochemical analyses of kidney biopsies from liver transplant recipients with chronic CsA nephrotoxicity showed significantly greater Nox2, α-SMA and picrosirius levels compared to controls.

**Conclusions—**These studies suggest that Nox2 is a modulator of CsA-induced hypoxia upstream of HIF-1α, and define the molecular characteristics that could be used for the diagnosis and monitoring of chronic CNI nephrotoxicity.

## Introduction

Calcineurin inhibitors (CNI) including CsA and tacrolimus are the cornerstone of maintenance immunosuppression in solid organ transplantation [1,2]. They play their immunosuppressive role by inhibiting the activity of calcineurin, a serine phosphatase that dephosphorylates nuclear factor of activated T cells (NFAT). Dephosphorylated NFAT translocates to the nucleus and induces the transcription of interleukin-2, an important cytokine for the activation and proliferation of T-lymphocytes [1]. Despite their beneficial actions in transplantation and many autoimmune disorders, the clinical use of CNIs is limited by their chronic nephrotoxicity [3–6]. This represents a significant clinical problem, as chronic CNI nephrotoxicity remains a dominant causative factor for kidney failure in nonkidney organ transplant recipients. Although non-specific, the pathological features of chronic CNI nephrotoxicity include progressive and irreversible interstitial fibrosis, tubular atrophy and arteriolar hyaline changes [3–6]. *De novo* or progressive arteriolar hyaline thickening (AH) is an important characteristic of chronic CNI nephrotoxicity [7].

Accumulating evidence suggests that chronic tubulointerstitial hypoxia is a final common pathway to end-stage renal disease [8–10]. CNIs result in decreased nitric oxide (NO) production and bioavailability, thereby leading to decreased vasodilation and unopposed vasoconstriction and hypoxia [5,8,11]. CNI-mediated arteriolopathy and narrowing of the arteriolar lumen contributes to the development of striped interstitial fibrosis, loss of peritubular capillaries, tubular atrophy and glomerular sclerosis [5,8]. In turn, hypoxia of the tubulointerstitial compartment may lead to the formation of free radicals or reactive oxygen species (ROS) causing cellular injury and death, promoting renal fibrosis, initiating a vicious cycle leading to end-stage renal disease [11–13]. A major limitation of studies addressing intrarenal oxygenation is the lack of noninvasive technologies to quantitate and monitor the bioavailability of oxygen in the kidney. Blood oxygen level-dependent MRI or BOLD MRI is an innovative imaging method that uses deoxyhemoglobin as an endogenous contrast

agent to determine tissue oxygen bioavailability [14]. Combining BOLD MRI with molecular assessment of renal hypoxia using biomarkers including Hypoxia Inducible Factor one alpha (HIF-1α) [15–17] and pimonidazole [18–20] represents an objective and global approach to the assessment of renal oxygenation.

NADPH oxidases are ubiquitous transmembrane proteins that generate superoxide ions ($O_2^-$) from molecular Oxygen ($O_2$) [21]. Unlike the other ROS producers, the seven isoforms of NADPH oxidases produce superoxide ions as their primary product rather than a metabolic byproduct. NADPH oxidase 2 (Nox2) was first discovered in macrophages where it plays a role in generating the ROS used in the oxidative killing of bacteria and fungi. It was later discovered in other organ systems including the kidney [22]. Deficiency of Nox2 is seen in individuals with chronic granulomatous disease and these patients suffer from recurrent infections mostly by catalase positive organisms including *S. aureus* and *A. fumigatus* [23].

A better understanding of the molecular mechanisms that regulate CNI-induced fibrosis will pave the way for the development of antifibrotic strategies [24]. Previous studies including from our group suggest that Nox2 regulates CNI-induced fibrogenesis in the kidney [25,26]. For these studies, we hypothesized that Nox2 is a modulator of CNI-induced renal hypoxia. Our objectives were to determine whether chronic treatment with CsA results in renal hypoxia, whether inhibition of Nox2 improves renal oxygenation, and whether liver transplant recipients on chronic CsA therapy have evidence of hypoxia in their kidneys.

## Materials and Methods

### Animal studies

Adult (9–11 week old) male Fisher 344 rats were purchased from Harlan (Madison, WI). Four to six week old wild type C57BL/6J (cat # 000664) and B6.129S-CybbTm1Din/J (cat # 2365) mice were purchased from Jackson Labs (Bar Harbor, Maine). Animals were housed in the animal care facility at the William S. Middleton VA Hospital in Madison, WI and all procedures were performed in accordance with the Animal Care Policies at the VA Hospital and the UW. All animals were placed on a 0.1% low salt diet (Teklad TD.94268) 1 week prior to treatment and for the duration of the experiments. Rats were randomized into four treatment groups: Castor oil vehicle, CsA (15mg/kg/day), CsA + diphenyleneiodonium (DPI, 0.5mg/kg/day), or CsA + Apocynin (16mg/kg/day). Apocynin and DPI are chemical inhibitors of Nox [25,27,28]. Castor, or olive oil is a classic vehicle for CsA used by others and our group, because CsA does not dissolve well in saline [25,29–34]. We have not observed any toxic effects of this vehicle in our studies. Six to eight rats were included in each experimental group. Doses were based on preliminary data and previous studies [25]. CsA and DPI were administered *i.p.* Apocynin was administered PO in the drinking water. Treatment was given for 1 month, and animals were euthanized by exsanguination under general anesthesia after BOLD MR imaging. Mice received intraperitoneal castor oil vehicle or CsA (30mg/kg/day). Animals were treated for 4–8 weeks for time course studies (6–10 animals in each group) and were euthanized after BOLD MR imaging 2 hours following pimonidazole. Creatinine levels were measured on IdexxVetTest 8008 bioanalyzer (Idexx Laboratories, West Sacramento, CA) using compatible assay chips.

### Immunohistochemistry and light microscopy

Immunohistochemical studies were performed as described previously [25,28,35]. H&E, PAS, trichrome, picrosirius red, Nox2, HSF, and α-SMA staining was performed using the concentrations outlined in the section below. Slides were imaged using a Nikon Eclipse E600 equipped with an Olympus DP70 camera or a Leica DMIL microscope equipped with Leica EC3 camera. Depending on the size of the stained section, either the entire section or 5 random non-overlapping images were taken for each section. Automated quantification was performed using a custom macro written for ImageJ software (NIH, imagej.nih.gov/ij/) as described previously [35].

### Immunoblot analyses

Protein extraction was performed as previously described using 20ug of protein [25,28,36,37]. The blots were incubated with primary antibody overnight at 4°C and with secondary antibodies for 1 hour at RT. HRP was visualized using West Femto chemiluminescence kit (Pierce, cat# 34095) and images were acquired using a Fotodyne imaging system (Harlan, WI).

### Antibodies and compounds

Nox2/gp91phox (1:250 for WB, 1:100 IHC, BD Biosciences, San Diego, CA, 611414), Nox4 (1:500, Santa Cruz, Dallas, TX, sc-21860), α-SMA (1:2000 for WB, 1:50,000 for IHC, Sigma, St. Louis, MO, A2547), HNE (1:1000, Abcam, Cambridge, MA, ab46545), GAPDH (1:5000, Abcam, ab8245), Vimentin (1:500, Bioss, Woburn, MA, bs-0756R), Beta Actin (1:7500, US Biological, Salem, MA), Fibronectin (1:400, Abcam, ab23750), Phospho-Smad2 (1:2500, Millipore, Billerica, MA, 04-953), Nitrotyrosine (1:750, Millipore, Billerica, MA, Ab5411), HIF-1 alpha (1:500, Thermo Fisher, Rockford, IL, PA3-16521), pimonidazole (1:100, Hypoxyprobe, Burlington, MA, HP2-200), Heat Shock Factor HSF (1:100, Enzo, Farmingdale, NY, ADI-SPA-950).

### BOLD MRI Studies

Rats and mice were scanned on a 3T GE scanner (GE Healthcare, Waukesha WI) with a wrist coil (rats) or a small animal coil (mice) using T2*-weighted multi-spoiled-gradient-recalled-echo sequence. Rats and mice were anesthetized with 1.5% isoflurane while breathing 100% O2, and were maintained above 35°C using a warm air blower. For the rats the sequence included 16 echoes, three slices with a 1 mm gap between each slice, and a 3 mm slice thickness in coronal and axial planes through the kidney). The following parameters were used: TR/TE/flip = 100ms/8–41.8ms/40°, BW = 62.5 kHz, FOV = 10–12 cm, and 256 x 256 matrix, NEX = 4. Each slice was acquired during free breathing. For mice, sequence included 6 echoes, two slices with a 0.5 mm gap between each slice, and a 6 mm slice thickness in coronal and axial planes through the kidney. The following parameters were used: TR/TE/flip/BW = 100ms/6.6–30ms/30°/±31.25; FOV = 6.0 cm and 256 x 256 matrix., NEX=16. Each slice is acquired during free breathing for both species. Image analysis was performed by generating R2* color maps and placing multiple region of interest (ROIs) in the cortex and medulla of each kidney using Functool® on the Advantage workstation (GE Healthcare, Waukesha WI). For mice, 2–3, and for rats, 3–5 non-

overlapping ROIs in the cortex and the outer medulla of either the coronal or axial image of the kidney were considered. The means for each animal were calculated for both the cortex and outer medulla. Mean cortical R2* values was obtained by averaging values from all ROIs in the cortex and mean medullary R2* was obtained by averaging values from all ROIs in the medulla.

### Perfusion MRI Studies

Evaluation of renal perfusion by dynamic contrast-enhanced MRI (DCE-MRI) was performed on a 1.5 T MRI scanner (Signa Excite, GE Healthcare, Waukesha, WI, USA) by use of a dedicated small animal coil. A paramagnetic contrast of Gd-DTPA (Multihance from Bracco Diagnostics Inc., Princeton, NJ, USA) was injected intravenously at a dose of 0.1 mmol/kg followed by a 1cc saline flush at a rate of 2cc/s. A T1-weighted fast 2D spoiled gradient echo (SPGR) sequence was used to acquire dynamic contrast-enhanced images of axial plane through the kidney. The following parameters were used for the perfusion acquisition: TR/TE/flip=5.8ms/2.8ms/15°, BW=125KHz, FOV=10–12cm, and 256 x 256 matrix. The images were acquired at a rate of 2 frame/s with a total of 200 frames taken in approximately 100s. Image analysis was performed by generating parametric maps of the area under the curve (AUC) from arrival to peak contrast enhancement (Initial AUC) [38–40] and the initial slope of the uptake of contrast to evaluate regional relative blood flow (rRBF). These measurements were performed by use of custom scripts written in Matlab (Matlab version 8.0, The MathWorks Inc., Cambridge, MA, USA).

### RNA extraction, purification and microarray analysis

RNA was extracted as previously described [28]. WT and Nox2−/− treated with vehicle or CsA for 8 weeks (n=4 in each group) were studied using the Affymetrix Mouse ST 2.0 microarray chips (Affymetrix, cat # 901169) and an Affymetrix GeneChip Analysis System. Mouse specific gene lists were generated from the rat genome database (rgd.mcw.edu) as described previously [35]. We identified gene group classifiers associated with injury-repair, metabolism, and OS-hypoxia. Analyses utilized Partek software, TAC software (Affymetrix) [41,42]. For tables 1 and 2, gene lists with p values < 0.05 were sorted and the top 40 genes with the highest p values were included. KEGG and Gene Ontology comparisons were utilized to determine pathways in which genes were involved and functions of the genes for grouping. TAC was used to create heat maps of the top genes.

### Hydrogen Peroxide (H2O2)

Serum H2O2 levels were measured using the Amplex Red Hydrogen Peroxide/Peroxidase Assay Kit from Molecular Probes, Invitrogen Corporation (Carlsbad, CA, # A-22188) as described previously [43]. The plate was read at 590nm using the SynergyTM HT Multi-Detection Microplate Reader and analyzed using the KC4 software (Bio-Tek, Winooski, VT). H2O2 concentrations were reported in μM.

### Patients

Liver transplant recipients on calcineurin inhibitors were selected if they had undergone an indication biopsy, had the histopathological diagnosis of chronic CsA nephrotoxicity

according to the Banff 2009 report and the arteriolar hyaline thickening-scoring scheme suggested by Sis et al [7], and had enough left-over tissue for processing and staining for our Nox2 studies. Because this was a proof of concept experiment, the first five patients that satisfied these criteria were selected. A second slide from each of the same subjects was provided and stained for Nox2 and α-SMA. Tissue staining was compared to normal tissue defined as pre-transplant donor kidney biopsies (n=5). These studies were performed in adherence to the Declaration of Helsinki and were approved by the Institutional Review Board at the University of Wisconsin School of Medicine and Public Health.

### Statistics

Student's T test and Mann-Whitney rank sum test were utilized as described previously [25,35] to compare parametric and non-parametric continuous data when appropriate. Similarly, Chi-square or Fisher's exact tests were utilized when appropriate to compare categorical data between groups. ANOVA was used to determine a p-value for each gene in the microarray by comparing the up- and down-regulation of the biological replicates in the comparison groups. Genes and other variables were considered significantly different if the p value was $< 0.05$. Graphs and statistical analyses were done using GraphPad Prism (GraphPad Software, La Jolla, CA).

## Results

### Nox2 inhibition prevented CsA induced hypoxia and OS in rats (Figures 1–6)

To assess whether Nox2 plays an important role in CsA-induced hypoxia and OS in rats, we first confirmed that 4 weeks of treatment with high-dose CsA resulted in reduced kidney function: serum creatinine (mg/dL) in the CsA group=0.54 ±0.20, vehicle=0.3±0.1, apocynin=0.48±0.1, DPI=0.5±0.1, p=0.04 between CsA and vehicle groups, and p=ns between CsA, and apocynin and DPI groups. We also confirmed the characteristic histopathological findings of arteriolar hyalinosis and striped fibrosis (Supplemental data, Figure 1). Next, immunoblot studies of whole kidney lysates showed an upregulation of biomarkers of OS (Nox2, HNE) and fibrogenesis (α-SMA, fibronectin, phosphorylated-Smad2) ($p < 0.05$ for all, Figure 1). To specifically evaluate renal oxygenation, we used BOLD MR imaging in animals treated with CsA, and with Nox2 inhibitors apocynin and DPI [25,27,28]. These studies demonstrated that CsA was associated with significant medullary ($R2^*=24\pm2$ vs. $16.2\pm1.5$, $p<0.05$) and cortical ($R2^*=16.3\pm1.3$ vs. $11.4\pm1.8$, $p<0.05$) hypoxia compared to vehicle (Figure 2). While prevention of CsA-induced hypoxia was not significant with apocynin, treatment with DPI reduced R2* levels significantly (cortex $10.4\pm1.4$ vs. $16.3\pm1.3$, $p<0.05$ and medulla $18.7\pm1.6$ vs. $24\pm2$, $p<0.05$), suggesting that Nox2 directly regulates CsA-induced renal hypoxia. To further assess the effect of Nox2 inhibition on OS and fibrogenesis, we conducted studies to assess Nox2, hydrogen peroxide, collagen, and vimentin expression. These studies demonstrated that apocynin and DPI were associated with downregulation of Nox2 expression by immunohistochemistry and western blot analyses ($p<0.05$ for CsA compared to all other groups, Figures 3-e, 5-b), serum hydrogen peroxide levels (vehicle 6.2±0.5, CsA 8.3±0.6, Apo-CsA 5.5±0.4, DPI-CsA 4.3±0.3 microM, $p<0.05$ for CsA compared to all groups, Figure 5-c), collagen by trichrome staining (Figure 4), and vimentin by immunoblot analyses (Figure 5).

### Nox2 knockout prevented CsA-induced hypoxia independent of regional perfusion (Figures 6–9)

To rigorously test our hypothesis we conducted similar experiments in wild type and Nox2−/− mice. Time course studies in wild type animals at 4 and 8 weeks demonstrated that CsA therapy resulted in cortical and medullary hypoxia as evidenced by increased R2* compared to vehicle (Figure 6). Importantly, CsA-induced hypoxia was significantly prevented in the medulla of Nox2−/− mice at 4 weeks (R2*=47±4.5 vs. 57.8±5, p=0.04), and in both cortex (R2*=34.9±4 vs. 39.8±3.8, p=0.009) and medulla (R2*=43.5±4 vs. 50.1±5, p=0.004) at 8 weeks, confirming the role of Nox2 in regulating CsA-induced hypoxia. To better understand the translation of hypoxia *in situ*, we used pimonidazole, a molecular marker of hypoxia that once delivered *in vivo*, binds to thiol groups at low oxygen tensions and can be visualized with commercially available anti-pimonidazole antibodies [18–20,44]. CsA therapy was associated with a significant increase in pimonidazole staining in the cortex (2.6±0.3 vs. 1.1±0.1, $p < 0.005$ compared to vehicle, and 2.6±0.3 vs. 1.6±0.2, $p < 0.05$ compared to KO), corticomedullary junction (1.6±0.2 vs. 0.8±0.1, $p < 0.005$ compared to vehicle, and 1.6±0.3 vs. 1.2±0.2, $p < 0.05$ compared to KO), and the medulla (1.3±0.1 vs. 0.2±0.1, $p < 0.005$ compared to vehicle, and 1.3±0.1 vs. 0.6±0.1, $p < 0.05$ compared to KO) of wild type mice (Figure 7). This staining was significantly reduced in Nox2−/− animals, confirming the BOLD MRI findings, and indicating that inhibiting Nox2 may prevent CsA-induced tubular hypoxia.

To determine whether CsA-induced hypoxia and the regulatory effect of Nox2 on were related to regional perfusion, we measured cortical and medullary perfusion with DCE imaging (Figure 8). Notably, these studies showed no significant differences related to CsA or Nox2, suggesting that the hypoxic effects of CsA and Nox2 are more likely related to microcirculation and cell metabolism than regional perfusion.

### Inhibition of CsA-induced hypoxia was associated with reduced fibrogenesis and OS (Figures 9–10)

To further characterize the role of Nox2 in CsA-induced renal injury, we performed immunoblot analyses examining matrix remodeling (vimentin), hypoxia (HIF-1α), and OS (HNE) at baseline and 8 weeks in vehicle and CsA-treated wild type and Nox2−/− mice (Figure 9). We observed reduced vimentin (1.05±0.1 vs. 0.8±0.1, p=0.02), HIF-1α (1.28±0.2 vs. 0.16±0.2, p=0.01), and HNE (0.7±0.1 vs. 0.37±0.2, p=0.02) levels in Nox2−/− animals compared to wild type. These studies were further validated as CsA-induced picrosirius red deposition was prevented in Nox2−/− animals (0.73±0.9 vs. 0.33±0.4, p=0.03 at 8 weeks, Figure 10), confirming that prevention of CsA-induced hypoxia is associated with reduced OS and fibrogenesis.

### Molecular signature of CsA nephrotoxicity (Figure 11, Tables 1, 2)

Our next objective was to identify the molecular signature of chronic CsA nephrotoxicity, and to characterize the effect of Nox2 on this phenotype. To date, there are no reliable and reproducible diagnostic criteria for chronic CNI nephrotoxicity in humans.

Table 1 and Figure 13 panel (a) display the top 40 genes with most significant p values, differentially expressed in kidneys from wild type mice treated with CsA compared to controls. These genes were sorted by p value from a pool of 410 transcripts, all differentially expressed, with a p value < 0.05 (Supplemental Table 1). Eighteen genes (45%) were upregulated whereas 22 genes (55%) were downregulated. Molecular classifiers defined primarily three groups (1) *injury-repair (18 genes)*, including molecules engaged in inflammation, immunity, cancer and development, (2) *metabolism (17 genes)* including molecules involved in transport, and (3) *OS-hypoxia (6 genes)*.

Table 2 displays the transcripts from Table 1 (shaded in grey) that were significantly affected in Nox2−/− animals treated with CsA. These transcripts were selected out of 2,693 differentially expressed transcripts observed comparing CsA treated wild type to Nox2−/− animals (Supplemental Table 2). The presence of Nox2 was associated with significantly higher levels of 4 genes (Vamp7, cwh43, Neat1, and capn6) and significantly reduced levels of the 4 remaining transcripts (Maob, Abcc4, Obox1, Igk), further characterizing the effect of Nox2 on transcript changes during chronic CsA nephrotoxicity.

### Nox2 was associated with CNI induced renal fibrosis in liver transplant recipients (Figure 12)

To assess the clinical relevance of these studies, we compared Nox2, α-SMA, heat shock factor (HSF), and picrosirius expression in clinical biopsies from liver transplant patients diagnosed with chronic CsA nephrotoxicity to pre-implantation biopsies from donor kidneys (Figure 12, n=5 in each group). These studies revealed higher tubulointerstitial expression of Nox2 (2.99±0.2 vs. 0.67±0.5, $p<0.05$) and α-SMA (6.1±0.5 vs. 1.7±0.2, $p<0.05$), and greater interstitial deposition of collagen noted by picrosirius staining (19±2 vs. 11.2±2, $p<0.05$).

## Discussion

Findings from this study suggest that Nox2 modulates chronic CsA-induced hypoxia independent of its effect on regional renal perfusion. Our observations from animal and clinical studies indicate that the absence of Nox2 prevents hypoxia, OS, and fibrogenesis following chronic CsA exposure and further validate Nox2 as a therapeutic target for prevention of chronic CNI nephrotoxicity [25]. Notably, we were able to define molecular classifiers in metabolism, injury-repair, and OS-hypoxia pathways that characterize chronic CsA nephrotoxicity. Although we have not completed in-depth analyses with tacrolimus, preliminary studies demonstrate that picrosirius red staining is similar in mice treated with tacrolimus (1mg/kg/24h) compared to CsA (data not shown).

Our findings are also consistent with previous reports demonstrating that Nox2 inhibition attenuates renal fibrosis resulting from ischemia reperfusion injury, chronic rejection, and CsA [25,28,35]. This time, we used noninvasive molecular imaging to demonstrate that chronic CsA was associated with hypoxia in the cortex and the medulla without a decline in corticomedullary perfusion. Blood oxygen level dependent magnetic resonance imaging is a noninvasive method to assess tissue oxygen bioavailability, using deoxyhemoglobin as an endogenous contrast agent [14,45,46]. This technique has been used to investigate human and

experimental models of kidney disease including aging [45,47], diabetes [48], acute and chronic allograft rejection [43,46,49], acute ischemic kidney injury and unilateral ureteral obstruction [50–52]. In contrast, dynamic contrast-enhanced imaging used to measure medullary and cortical perfusion [38–40] did not detect significant hypoperfusion or changes related to CsA or Nox2. Together with observations from our molecular studies, these findings suggest that the effects of CsA and Nox2 are more likely related to active renal metabolism and microcirculation injury. Our recent understanding of endothelial, epithelial, and inflammatory cell interactions indicates that the initial injury (ischemic, toxic, obstructive, or alloimmune) to epithelial and endothelial cells triggers signaling cascades of local inflammatory mediators that induce local injury and recruitment of professional inflammatory cells including PMNs, macrophages, NK, and B cells. This recruitment results in adaptive or maladaptive responses leading to tissue repair, or terminal fibrosis and microvascular rarefaction [53,54]. Early tissue hypoxia is a result of microcirculation injury and hypoperfusion due to endothelial cell swelling, RBC rouleaux formation, platelet aggregation, and activation of the coagulation and complement cascades, which results in the activation of HIF response pathway, an oxygen response system that has been used as a molecular marker of renal hypoxia [15–17,55]. HIF molecules are regulated at the protein level by oxygen-dependent enzymes, and play a central role in the adaptation of metabolism to hypoxia. Specifically, the activation of HIF-1α by hypoxia results in a change in cellular metabolism from oxidative phosphorylation to anaerobic glycolysis by increasing the expression of glycolytic enzymes, blocking the conversion of pyruvate to acetyl CoA, and regulating the expression of proteins that compose the mitochondrial respiratory chain [55–59].

Consistent with this hypothesis, our observations suggest that Nox2 regulates HIF, pointing to a more pervasive role for this Nox enzyme than its classically defined effect in phagocytes. Although cellular responses to low oxygen tension have been studied extensively, mechanisms underlying these functions are still unclear. HIFs in the presence of hypoxic oxygen levels are activated through a complex mechanism in which the oxygen tension is critical and bind to hypoxia-responsive elements, activating the transcription of more than two hundred genes that allow cells to adapt to hypoxia [16,17]. Findings from this study indicate that Nox2 is an upstream activator of HIF and OS, playing an important role in the regulation of metabolic and solute carrier pathways, which also need oxygen to operate.

Current knowledge regarding the accurate diagnosis of chronic CNI nephrotoxicity is limited. *De novo* or progressive arteriolar hyaline thickening may be the most pathognomonic lesion of chronic CNI nephrotoxicity [7,29]. This lesion consists of vacuolization of endothelial and smooth muscle cells, and focal or circular lumpy protein deposits in the arteriolar wall, which usually replace necrotic smooth muscle cells and eventually narrow the vascular lumen[7]. Inter-observer variation for this lesion is high however, and probably not only related to the method used but also may be partly explained by the focal and patchy nature of the arteriolar lesions or by the variation of severity of damage from one arteriole to the other, which makes the examination of every arteriole in the renal biopsy crucial [7]. In addition, there is substantial risk in the community to over-diagnose chronic CNI nephrotoxicity using current diagnostic standards. As a result, providers may reduce CNI exposure and expose patients to a higher possibility of antibody-

mediated rejection and late graft loss [60,61]. It is therefore important to define reliable molecular diagnostic tools for CNI-induced renal injury. Our study identified a list of 40 transcripts that were primarily involved in metabolism, oxidative stress, and tissue injury-repair.

Our study is limited by the sample size of liver transplant recipients with chronic CNI nephrotoxicity and the absence of a control group of liver transplant recipients without chronic CNI therapy. However, the control group of pretransplant donor biopsies provides an alternative, and the proof of concept to support our hypothesis. In conclusion, these data suggest that molecular classifiers may be used for the diagnosis and monitoring of chronic CNI nephrotoxicity, and further delineate the role of Nox2 in CsA-induced renal hypoxia as a mediator of HIF signaling and metabolic pathways that regulate OS, cell transport, and injury-repair.

## Supplementary Material

Refer to Web version on PubMed Central for supplementary material.

## Acknowledgments

Funding. Funding for this project was provided by the NIDDK grant (5R01DK092454-04).

## Abbreviations

| | |
|---|---|
| **4-HNE** | 4 hydroxynonenal |
| **AH** | arteriolar hyaline thickening |
| **α-SMA** | Alpha smooth muscle actin |
| **AUC** | Area under the curve |
| **BOLD MRI** | Blood Oxygen Level Dependent Magnetic Resonance Imaging |
| **CNI** | Calcineurin inhibitors |
| **CsA** | Cyclosporine A |
| **DPI** | diphenyleneiodonium |
| **DCE MRI** | Dynamic contrast-enhanced MRI |
| **ESRD** | End stage renal disease |
| **GAPDH** | glyceraldehyde-3-phosphate dehydrogenase |
| **HRP** | Horseradish peroxidase |
| **HSF** | Heat Shock Factor |
| **HIF-1α** | Hypoxia Inducible Factor one alpha |
| **H2O2** | Hydrogen Peroxide |
| **IHC** | Immunohistochemistry |

| | |
|---|---|
| **NFAT** | Nuclear factor of activated T cells |
| **NADPH** | Reduced Nicotinamide adenosine diphosphate |
| **NO** | Nitric Oxide |
| **Nox** | NADPH oxidase |
| **OS** | Oxidative Stress |
| **rRBF** | regional relative blood flow |
| **ROS** | Reactive Oxygen Species |

## References


1. Samaniego M, Becker BN, Djamali A. Drug insight: maintenance immunosuppression in kidney transplant recipients. Nat Clin Pract Nephrol. 2006; 2(12):688–699. [PubMed: 17124526]
2. Flechner SM, Kobashigawa J, Klintmalm G. Calcineurin inhibitor-sparing regimens in solid organ transplantation: focus on improving renal function and nephrotoxicity. Clin Transplant. 2008; 22(1): 1–15. [PubMed: 18217899]
3. Liptak P, Ivanyi B. Primer: Histopathology of calcineurin-inhibitor toxicity in renal allografts. Nat Clin Pract Nephrol. 2006; 2(7):398–404. quiz following 404. [PubMed: 16932468]
4. Olyaei AJ, de Mattos AM, Bennett WM. Nephrotoxicity of immunosuppressive drugs: new insight and preventive strategies. Curr Opin Crit Care. 2001; 7(6):384–389. [PubMed: 11805539]
5. Naesens M, Kuypers DR, Sarwal M. Calcineurin inhibitor nephrotoxicity. Clin J Am Soc Nephrol. 2009; 4(2):481–508. [PubMed: 19218475]
6. Ojo AO. Renal disease in recipients of nonrenal solid organ transplantation. Semin Nephrol. 2007; 27(4):498–507. [PubMed: 17616280]
7. Sis B, Dadras F, Khoshjou F, Cockfield S, Mihatsch MJ, Solez K. Reproducibility studies on arteriolar hyaline thickening scoring in calcineurin inhibitor-treated renal allograft recipients. Am J Transplant. 2006; 6(6):1444–1450. [PubMed: 16686769]
8. Nangaku M. Chronic hypoxia and tubulointerstitial injury: a final common pathway to end-stage renal failure. J Am Soc Nephrol. 2006; 17(1):17–25. [PubMed: 16291837]
9. Eckardt KU, Bernhardt WM, Weidemann A, et al. Role of hypoxia in the pathogenesis of renal disease. Kidney Int Suppl. 2005; (99):S46–S51. [PubMed: 16336576]
10. Manotham K, Tanaka T, Matsumoto M, et al. Evidence of tubular hypoxia in the early phase in the remnant kidney model. J Am Soc Nephrol. 2004; 15(5):1277–1288. [PubMed: 15100368]
11. Zhong Z, Arteel GE, Connor HD, et al. Cyclosporin A increases hypoxia and free radical production in rat kidneys: prevention by dietary glycine. Am J Physiol. 1998; 275(4 Pt 2):F595–604. [PubMed: 9755131]
12. Krauskopf A, Lhote P, Petermann O, Ruegg UT, Buetler TM. Cyclosporin A generates superoxide in smooth muscle cells. Free Radic Res. 2005; 39(9):913–919. [PubMed: 16087472]
13. Djamali A. Oxidative Stress as a Common Pathway to Chronic Tubulointerstitial Injury in Kidney Allografts. Am J Physiol Renal Physiol. 2007; 293(2):F445–455. [PubMed: 17459952]
14. Prasad PV, Edelman RR, Epstein FH. Noninvasive evaluation of intrarenal oxygenation with BOLD MRI. Circulation. 1996; 94(12):3271–3275. [PubMed: 8989140]
15. Rosenberger C, Pratschke J, Rudolph B, et al. Immunohistochemical Detection of Hypoxia-Inducible Factor-1{alpha} in Human Renal Allograft Biopsies. J Am Soc Nephrol. 2007; 18(1): 343–351. [PubMed: 17182883]
16. Maxwell P. HIF-1: an oxygen response system with special relevance to the kidney. J Am Soc Nephrol. 2003; 14(11):2712–2722. [PubMed: 14569080]
17. Semenza GL. HIF-1, O(2), and the 3 PHDs: how animal cells signal hypoxia to the nucleus. Cell. 2001; 107(1):1–3. [PubMed: 11595178]

18. Westbury CB, Pearson A, Nerurkar A, et al. Hypoxia can be detected in irradiated normal human tissue: a study using the hypoxic marker pimonidazole hydrochloride. Br J Radiol. 2007; 80(959): 934–938. [PubMed: 17908818]
19. Yaromina A, Zips D, Thames HD, et al. Pimonidazole labelling and response to fractionated irradiation of five human squamous cell carcinoma (hSCC) lines in nude mice: the need for a multivariate approach in biomarker studies. Radiother Oncol. 2006; 81(2):122–129. [PubMed: 16956683]
20. Kaanders JH, Wijffels KI, Marres HA, et al. Pimonidazole binding and tumor vascularity predict for treatment outcome in head and neck cancer. Cancer Res. 2002; 62(23):7066–7074. [PubMed: 12460928]
21. Bedard K, Krause KH. The NOX family of ROS-generating NADPH oxidases: physiology and pathophysiology. Physiol Rev. 2007; 87(1):245–313. [PubMed: 17237347]
22. Gill PS, Wilcox CS. NADPH oxidases in the kidney. Antioxid Redox Signal. 2006; 8(9–10):1597–1607. [PubMed: 16987014]
23. Battersby AC, Cale CM, Goldblatt D, Gennery AR. Clinical Manifestations of Disease in X-Linked Carriers of Chronic Granulomatous Disease. Journal of Clinical Immunology. 2013; 33(8): 1276–1284. [PubMed: 24078260]
24. Liu Y. New insights into epithelial-mesenchymal transition in kidney fibrosis. J Am Soc Nephrol. 21(2):212–222. [PubMed: 20019167]
25. Djamali A, Reese S, Hafez O, et al. Nox2 is a mediator of chronic CsA nephrotoxicity. Am J Transplant. 2012; 12(8):1997–2007. [PubMed: 22568654]
26. Reddy RN, Knotts TL, Roberts BR, Molkentin JD, Price SR, Gooch JL. Calcineurin A-beta is required for hypertrophy but not matrix expansion in the diabetic kidney. J Cell Mol Med. 2011; 15(2):414–422. [PubMed: 19778355]
27. Aldieri E, Riganti C, Polimeni M, et al. Classical Inhibitors of NOX NAD(P)H Oxidases Are Not Specific. Curr Drug Metab. 2008; 9(8):686–696. [PubMed: 18855607]
28. Djamali A, Vidyasagar A, Adulla M, Hullett D, Reese S. Nox-2 Is a Modulator of Fibrogenesis in Kidney Allografts. Am J Transplant. 2009; 9(1):74–82. [PubMed: 18976289]
29. Young BA, Burdmann EA, Johnson RJ, et al. Cyclosporine A induced arteriolopathy in a rat model of chronic cyclosporine nephropathy. Kidney Int. 1995; 48(2):431–438. [PubMed: 7564110]
30. Carlos CP, Mendes GE, Miquelin AR, et al. Macrophage depletion attenuates chronic cyclosporine A nephrotoxicity. Transplantation. 2010; 89(11):1362–1370. [PubMed: 20535850]
31. Yang CW, Faulkner GR, Wahba IM, et al. Expression of apoptosis-related genes in chronic cyclosporine nephrotoxicity in mice. Am J Transplant. 2002; 2(5):391–399. [PubMed: 12123203]
32. Nagatoya K, Moriyama T, Kawada N, et al. Y-27632 prevents tubulointerstitial fibrosis in mouse kidneys with unilateral ureteral obstruction. Kidney Int. 2002; 61(5):1684–1695. [PubMed: 11967018]
33. Yang CW, Ahn HJ, Kim WY, et al. Synergistic effects of mycophenolate mofetil and losartan in a model of chronic cyclosporine nephropathy. Transplantation. 2003; 75(3):309–315. [PubMed: 12589150]
34. Reese SR, Wilson NA, Huang G, Redfield RR 3rd, Zhong W, Djamali A. Calcineurin Inhibitor Minimization With Ixazomib, an Investigational Proteasome Inhibitor, for the Prevention of Antibody Mediated Rejection in a Preclinical Model. Transplantation. 2015; 99(9):1785–1795. [PubMed: 25919767]
35. Karim AS, Reese SR, Wilson NA, Jacobson LM, Zhong W, Djamali A. Nox2 Is a Mediator of Ischemia Reperfusion Injury. Am J Transplant. 2015; 15(11):2888–2899. [PubMed: 26104383]
36. Vidyasagar A, Reese S, Acun Z, Hullett D, Djamali A. HSP27 is involved in the pathogenesis of kidney tubulointerstitial fibrosis. Am J Physiol Renal Physiol. 2008; 295(3):F707–716. [PubMed: 18596079]
37. Kiernan, JA. Histological and histochemical methods: theory and practice. 3. London England; New York: Arnold; 1999.
38. Evelhoch JL. Key factors in the acquisition of contrast kinetic data for oncology. J Magn Reson Imaging. 1999; 10(3):254–259. [PubMed: 10508284]

39. Simpson NE, He Z, Evelhoch JL. Deuterium NMR tissue perfusion measurements using the tracer uptake approach: I. Optimization of methods. Magn Reson Med. 1999; 42(1):42–52. [PubMed: 10398949]
40. Simpson NE, Evelhoch JL. Deuterium NMR tissue perfusion measurements using the tracer uptake approach: II. Comparison with microspheres in tumors. Magn Reson Med. 1999; 42(2):240–247. [PubMed: 10440948]
41. Huang da W, Sherman BT, Lempicki RA. Bioinformatics enrichment tools: paths toward the comprehensive functional analysis of large gene lists. Nucleic Acids Res. 2009; 37(1):1–13. [PubMed: 19033363]
42. Huang da W, Sherman BT, Lempicki RA. Systematic and integrative analysis of large gene lists using DAVID bioinformatics resources. Nat Protoc. 2009; 4(1):44–57. [PubMed: 19131956]
43. Djamali A, Sadowski E, Muehrer R, et al. BOLD-MRI assessment of Intrarenal Oxygenation and Oxidative Stress in Patients with Chronic Kidney Allograft Dysfunction. Am J Physiol Renal Physiol. 2007; 292(2):F513–F522. [PubMed: 17062846]
44. Varia MA, Calkins-Adams DP, Rinker LH, et al. Pimonidazole: a novel hypoxia marker for complementary study of tumor hypoxia and cell proliferation in cervical carcinoma. Gynecol Oncol. 1998; 71(2):270–277. [PubMed: 9826471]
45. Prasad PV, Epstein FH. Changes in renal medullary pO2 during water diuresis as evaluated by blood oxygenation level-dependent magnetic resonance imaging: effects of aging and cyclooxygenase inhibition. Kidney Int. 1999; 55(1):294–298. [PubMed: 9893139]
46. Djamali A, Sadowski EA, Samaniego-Picota M, et al. Noninvasive assessment of early kidney allograft dysfunction by blood oxygen level-dependent magnetic resonance imaging. Transplantation. 2006; 82(5):621–628. [PubMed: 16969284]
47. Epstein FH, Prasad P. Effects of furosemide on medullary oxygenation in younger and older subjects. Kidney Int. 2000; 57(5):2080–2083. [PubMed: 10792627]
48. Epstein FH, Veves A, Prasad PV. Effect of diabetes on renal medullary oxygenation during water diuresis. Diabetes Care. 2002; 25(3):575–578. [PubMed: 11874950]
49. Sadowski EA, Fain SB, Alford SK, et al. Assessment of Acute Renal Transplant Rejection with Blood Oxygen Level-Dependent MR Imaging: Initial Experience. Radiology. 2005; 236(3):911–919. [PubMed: 16118170]
50. Alford SK, Sadowski EA, Unal O, et al. Detection of acute renal ischemia in swine using blood oxygen level-dependent magnetic resonance imaging. J Magn Reson Imaging. 2005; 22(3):347–353. [PubMed: 16104014]
51. Pedersen M, Dissing TH, Morkenborg J, et al. Validation of quantitative BOLD MRI measurements in kidney: application to unilateral ureteral obstruction. Kidney Int. 2005; 67(6): 2305–2312. [PubMed: 15882272]
52. Juillard L, Lerman LO, Kruger DG, et al. Blood oxygen level-dependent measurement of acute intra-renal ischemia. Kidney Int. 2004; 65(3):944–950. [PubMed: 14871414]
53. Legrand M, Mik EG, Johannes T, Payen D, Ince C. Renal hypoxia and dysoxia after reperfusion of the ischemic kidney. Mol Med. 2008; 14(7–8):502–516. [PubMed: 18488066]
54. Molitoris BA. Therapeutic translation in acute kidney injury: the epithelial/endothelial axis. J Clin Invest. 2014; 124(6):2355–2363. [PubMed: 24892710]
55. Haase VH. Mechanisms of hypoxia responses in renal tissue. J Am Soc Nephrol. 2013; 24(4):537–541. [PubMed: 23334390]
56. Hamaguchi T, Iizuka N, Tsunedomi R, et al. Glycolysis module activated by hypoxia-inducible factor 1alpha is related to the aggressive phenotype of hepatocellular carcinoma. Int J Oncol. 2008; 33(4):725–731. [PubMed: 18813785]
57. Formenti F, Constantin-Teodosiu D, Emmanuel Y, et al. Regulation of human metabolism by hypoxia-inducible factor. Proc Natl Acad Sci U S A. 2010; 107(28):12722–12727. [PubMed: 20616028]
58. Weinberg JM. Mitochondrial biogenesis in kidney disease. J Am Soc Nephrol. 2011; 22(3):431–436. [PubMed: 21355058]
59. Semenza GL. Regulation of metabolism by hypoxia-inducible factor 1. Cold Spring Harb Symp Quant Biol. 2011; 76:347–353. [PubMed: 21785006]

60. Gaston RS, Cecka JM, Kasiske BL, et al. Evidence for antibody-mediated injury as a major determinant of late kidney allograft failure. Transplantation. 2010; 90(1):68–74. [PubMed: 20463643]

61. Gaston RS. Chronic calcineurin inhibitor nephrotoxicity: reflections on an evolving paradigm. Clin J Am Soc Nephrol. 2009; 4(12):2029–2034. [PubMed: 19850771]

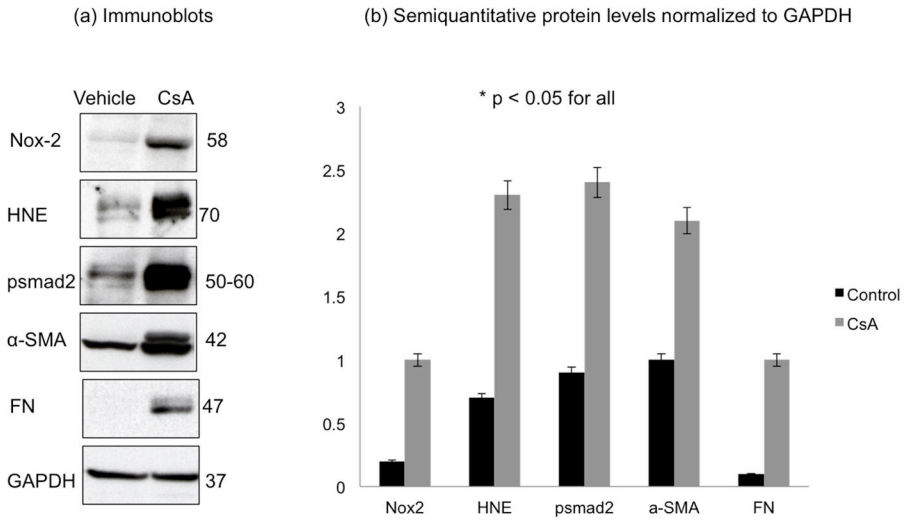


**Figure 1. CsA toxicity was associated with fibrogenesis and OS in rats**

CsA toxicity was associated with fibrogenesis and OS in rats. Immunoblot analyses of whole kidney tissue lysates from rats treated with CsA or vehicle for 1 month. Panel (a) shows representative blots and Panel (b) represents the semiquantitative assessment of all protein expression normalized to GAPDH with Image J software analyses using the mean of three representative blots from three different animals. These studies determined an upregulation of biomarkers of oxidative stress (Nox2, Nox4, p22phox, HNE) and fibrogenesis (α-SMA, fibronectin, phosphorylated-Smad2).

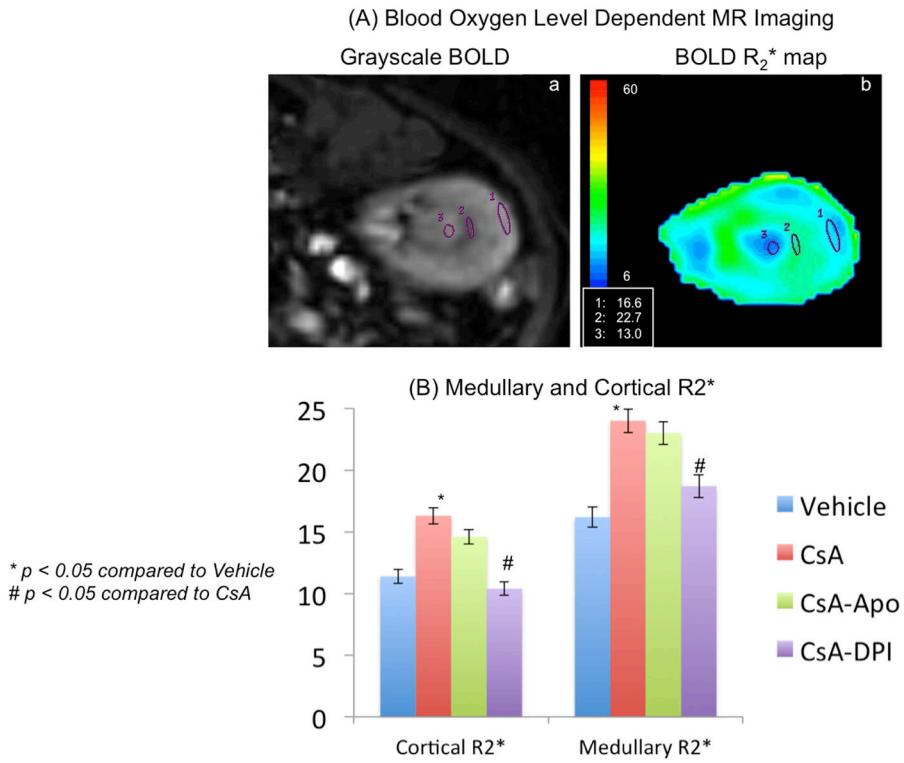


**Figure 2. Nox2 inhibition prevented CsA-induced hypoxia in rats-BOLD MRI studies**

Nox2 inhibition prevented CsA-induced hypoxia in rats-BOLD MRI studies. Adult male Fisher 344 rats were randomized into four treatment groups: Castor oil vehicle, Cyclosporine (15mg/kg/day) alone, Cyclosporine (15mg/kg/day) + diphenyleneiodonium (DPI, 0.5mg/kg/day), or Cyclosporine (15mg/kg/day) + Apocynin (16mg/kg/day) (n=6–8 in each treatment group). Panel (A) represents Grayscale and BOLD color map images of a control rat kidney. The color map indicates the cortex and inner medullar have lower R2* values (1,3) than the outer medulla (2). Panel (B) displays the bar graph of mean (±SD) cortical and medullary R2* levels in the 4 treatment groups. CsA therapy resulted in a significant increase in R2* levels indicating cortical and medullary hypoxia. Co-treatment with DPI prevented cortical and medullary hypoxia (significantly lower R2* levels). Therapy with Apocynin did not result in a significant change in R2* levels.

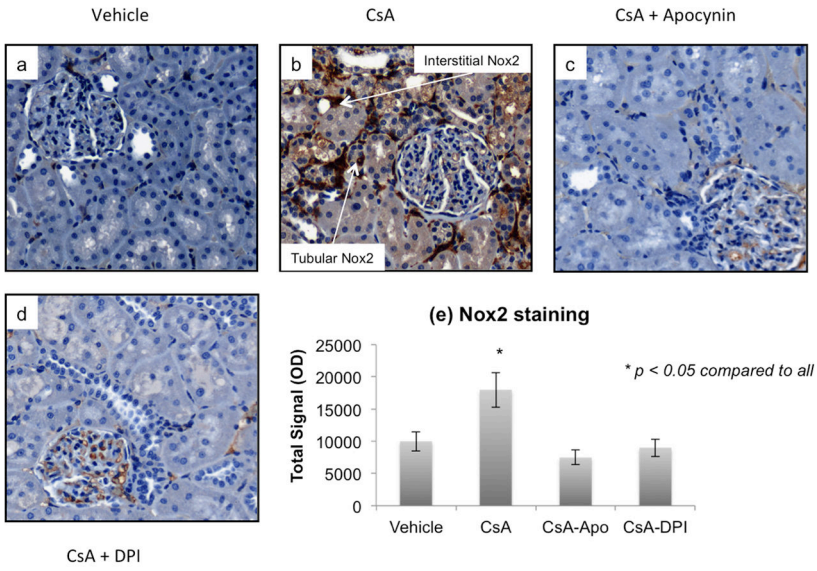


**Figure 3. Apocynin and DPI prevented CsA-induced Nox2 expression in rats**

Apocynin and DPI prevented CsA-induced Nox2 expression in rats. Panels a-d display representative images of Nox2 staining experiments in rats treated with castor oil, CsA, CsA-Apocynin and CsA-DPI (n=6–8 in each group). Panel e represents the semiquantitative assessment of Nox2 staining using digital software analyses. The studies showed that CsA upregulated Nox2 expression in renal cortical tubules and interstitium. Nox2 expression was significantly inhibited by apocynin and DPI.

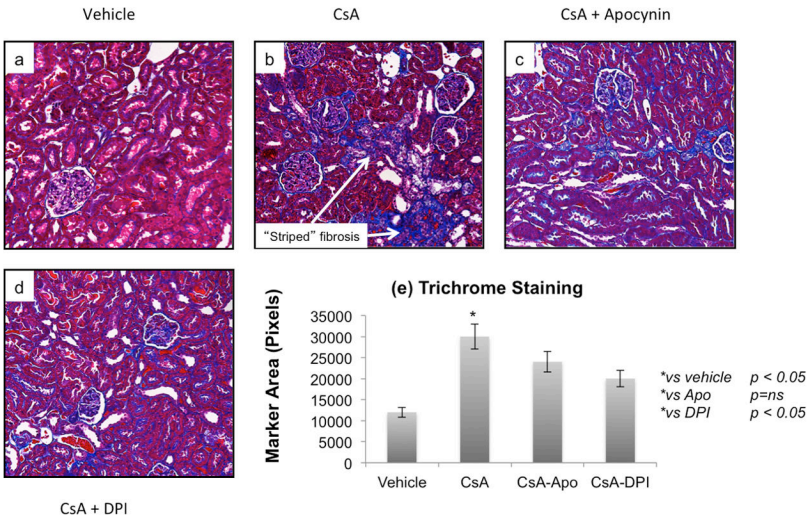


**Figure 4. Nox2 inhibition prevented CsA-induced fibrosis in rats**

Nox2 inhibition prevented CsA-induced fibrosis in rats. Panels a-d display representative images of trichrome blue staining experiments in rats treated with castor oil, CsA, CsA-Apocynin and CsA-DPI (n=6–8 in each group). Panel e represents the semiquantitative assessment of trichrome blue using digital software analyses. The studies showed that CsA increased interstitial trichrome staining compared to control. Fibrosis was significantly inhibited by DPI, while apocynin-associated changes did not reach statistical significance.

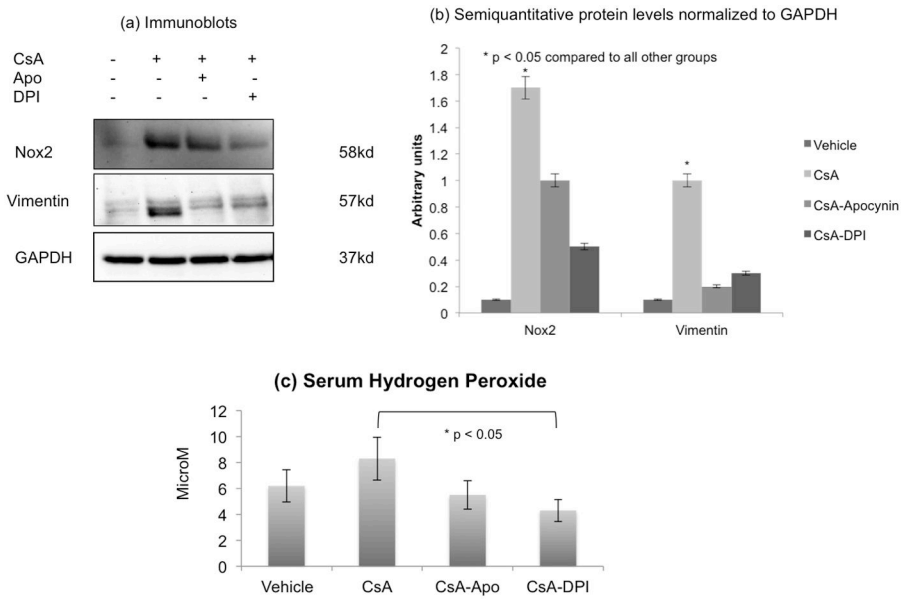


**Figure 5. Apocynin and DPI prevented CsA-induced fibrosis and OS in rats**

Apocynin and DPI prevented CsA-induced fibrosis and OS in rats. Panel a displays representative immunoblots of Nox2, vimentin, and GAPDH internal control from whole kidney tissue lysates from rats treated with castor oil, CsA, CsA-Apocynin and CsA-DPI. Panel b represents the semiquantitative assessment of Nox2 and vimentin expression normalized to GAPDH with Image J software analyses using the mean of three representative blots from three different rats. Panel c displays serum hydrogen peroxide measurements using the Amplex Red assay. The studies showed that CsA upregulation of Nox2 and vimentin protein levels was blunted by apocynin and DPI (Panels a,b). Similarly, the increase in systemic hydrogen peroxide levels (H2O2) was prevented by DPI. Apocynin related changes did not reach statistical significance (Panel c).

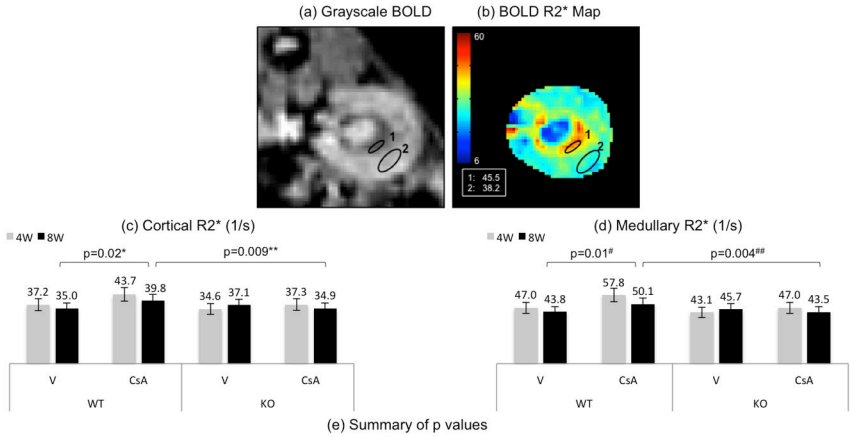


(e) Summary of p values

| | | | 4 Weeks (4W) | 8 Weeks (8W) |
|---|---|---|---|---|
| Cortical R2* | WT | CsA vs. V | 0.05 | 0.02* |
| | WT vs. KO | V | 0.04 | 0.5 |
| | | CsA | 0.2 | 0.009** |
| | KO | CsA vs. V | 0.03 | 0.4 |
| Medullary R2* | WT | CsA vs. V | 0.002 | 0.01# |
| | WT vs. KO | V | 0.05 | 0.5 |
| | | CsA | 0.04 | 0.004## |
| | KO | CsA vs. V | 0.02 | 0.4 |

**Figure 6. Nox2$^{-/-}$ prevented CsA-induced intrarenal hypoxia in mice-BOLD MRI Studies**

Nox2$^{-/-}$ prevented CsA-induced intrarenal hypoxia in mice-BOLD MRI Studies. CsA (30mg/kg/day) was administered i.p. to C57BL/6J mice and B6.129S-CybbTm1Din/J (Nox2−/−) mice. Animals were treated for 4–8 weeks for time course studies (6–10 animals in each group). BOLD MRI grayscale gradient echo anatomical image (Panel a) with correlative color R2* map (Panel b). The color map indicates the cortex has a lower R2* values (2) than the outer medulla (1). Panels c and d display bar graphs of mean cortical and medullary R2* levels at 4 and 8 weeks in control and CsA treated wild type and Nox2−/− mice. Panel e is a Table summarizing the p values for the difference between various groups. CsA therapy in wild type animals resulted in cortical and medullary hypoxia as evidenced by increased R2* compared to vehicle (Panels c,d,e). CsA therapy had no significant effect on intrarenal oxygenation in Nox2−/− animals compared to vehicle at 8 weeks. CsA-induced hypoxia was significantly prevented in the cortex and medulla of Nox2−/− mice at 8 weeks (Panels c,d,e).

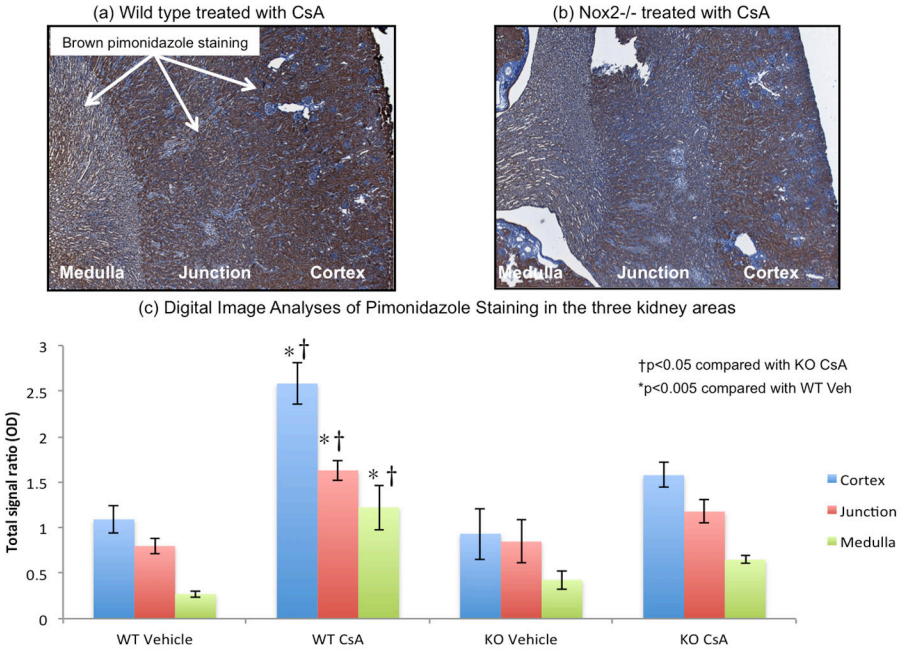


**Figure 7. Nox2$^{-/-}$ prevented CsA-induced intrarenal hypoxia measured by pimonidazole**

Nox2$^{-/-}$ prevented CsA-induced intrarenal hypoxia measured by pimonidazole. Animals received pimonidazole *i.p.* (60mg/kg) 2 hours prior to terminal exsanguination. Panels and b display representative pimonidazole staining (brown color) in wild type (a) and Nox2−/− mice (b). Intensity of staining is greater in panel (a) and the distinction between cortex and outer medulla is not as clear in wild type animals as in Nox2−/− mice. Panel c is a bar graph representing semiquantitative pimonidazole staining intensity in the 4 groups using digital software analyses (n=6–10 in each group). These studies determined that CsA therapy was associated with a significant increase in pimonidazole staining in wild type mice. However, this staining was significantly reduced in Nox2−/− animals, to baseline control levels.

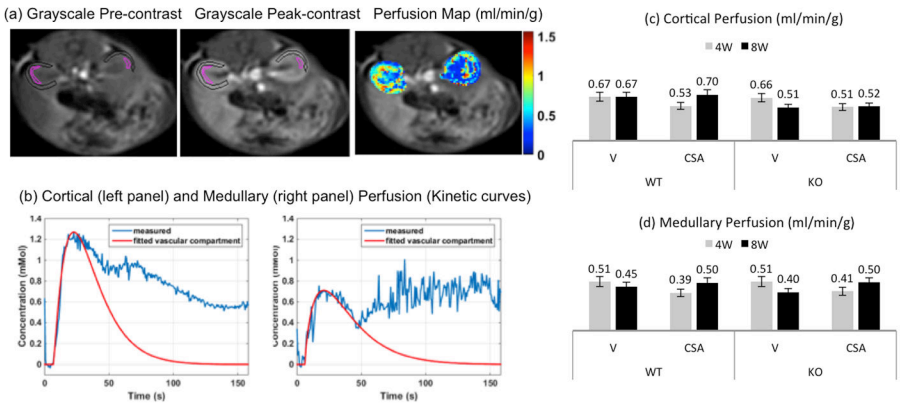


(e) Summary of p values

| | | | p values | |
|---|---|---|---|---|
| | | | 4W | 8W |
| Cortical Perfusion | WT v KO | V | 0.90 | 0.68 |
| | | CsA | 0.87 | 0.06 |
| | WT | V v CsA | 0.24 | 0.80 |
| | KO | V v CsA | 0.26 | 0.82 |
| Medullary Perfusion | WT v KO | V | 1.00 | 0.68 |
| | | CsA | 0.84 | 0.99 |
| | WT | V v CsA | 0.24 | 0.80 |
| | KO | V v CsA | 0.26 | 0.48 |

**Figure 8. Renal Perfusion was not affected by CsA or Nox2**

Regional perfusion was not affected by CsA and Nox2. Using DCE imaging, we fit the renal contrast uptake as a single, first pass vascular compartment for this analysis. This gave the best separation between the groups. We used an average arterial input function (AIF) calculated from each mouse. Panel (a) shows grayscale pre-contrast and peak-contrast, and perfusion color map (ml/min/g) images in a control mouse at baseline. Panel (b) shows measured and fitted vascular compartment kinetic maps in cortex and medulla. Panels (c) and (d) represent bar graphs of renal cortical and medullary perfusion of experimental animals at baseline, 4W, and 8W. These studies showed no significant effect of CsA or Nox2 on regional perfusion. Panel (e) is a summary table of the p values comparing perfusion values.

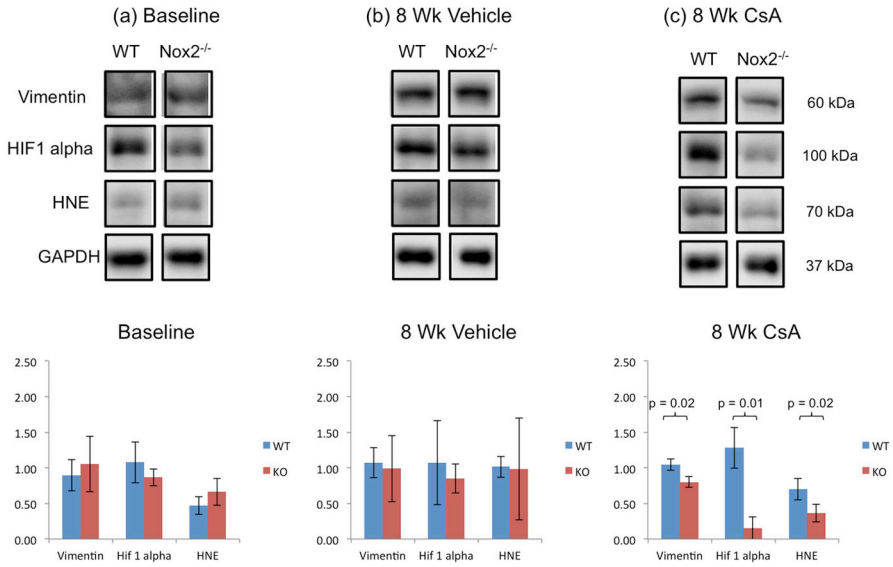


**Figure 9. Nox2$^{-/-}$ prevented CsA-induced Fibrogenesis and OS in mice**

Nox2$^{-/-}$ prevented CsA-induced Fibrogenesis and OS in mice. We performed immunoblot analyses examining matrix remodeling (vimentin), hypoxia (HIF-1α), and OS (HNE) at baseline and 8 weeks in vehicle and CsA-treated wild type and Nox2−/− mice. We observed reduced vimentin, HIF-1α, and HNE levels in Nox2−/− animals compared to wild type. Bar graphs represent semiquantitative assessment of protein expression normalized to GAPDH with Image J software analyses using the mean of three representative blots from three different mice at baseline, 8 wks vehicle and 8 wks CsA groups.

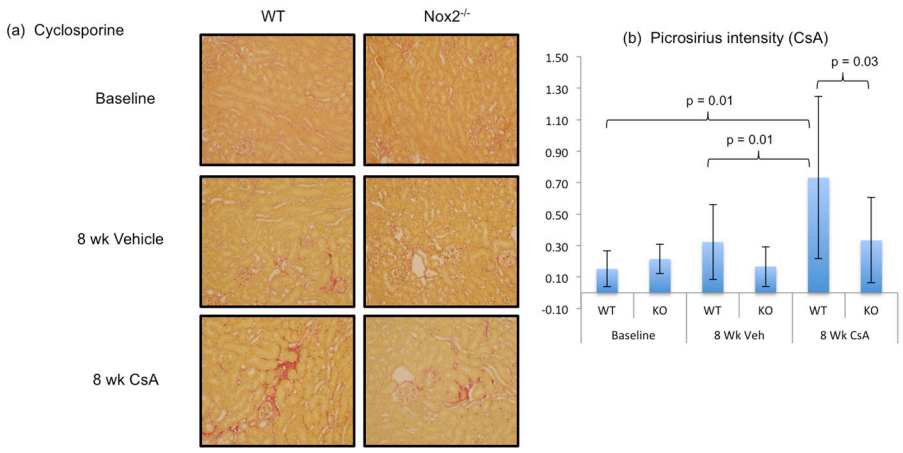


**Figure 10. CsA-induced picrosirius red staining was prevented in Nox2−/− mice**

CsA-associated picrosirius staining was prevented in Nox2−/− mice. High dose CsA (15 mg/kg/d x 8 weeks) resulted in significantly greater collagen deposition measured by picrosirius digital quantification (Panels a–d). Picrosirius staining was significantly reduced in CsA treated Nox2−/− animals (Panels a, and b).

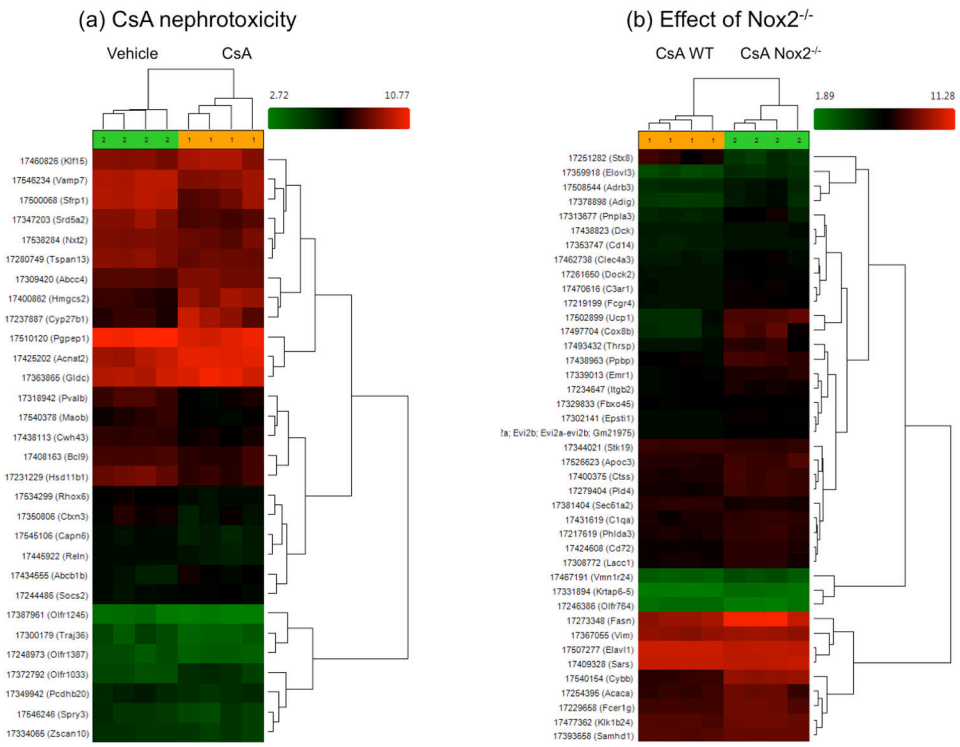


**Figure 11. Molecular classifiers defining the top 40 genes characterizing CsA nephrotoxicity in mice and the effect of Nox2$^{-/-}$ on CsA nephrotoxicity**

Molecular classifiers defining the top 40 genes characterizing CsA nephrotoxicity in mice and the effect of Nox2$^{-/-}$ on CsA nephrotoxicity. Heat maps displaying the top 40 genes with most significant p values, differentially expressed in kidneys from wild type mice treated with CsA compared to controls. These genes were isolated out of a pool of 410 transcripts, all differentially expressed, with a p value < 0.05 (Panel a). Panel b displays the top 40 genes (out of 662 significantly different transcripts) characterizing the molecular effect of Nox2 on chronic CsA nephrotoxicity. Most (85%) of these transcripts were decreased in the absence of Nox2.

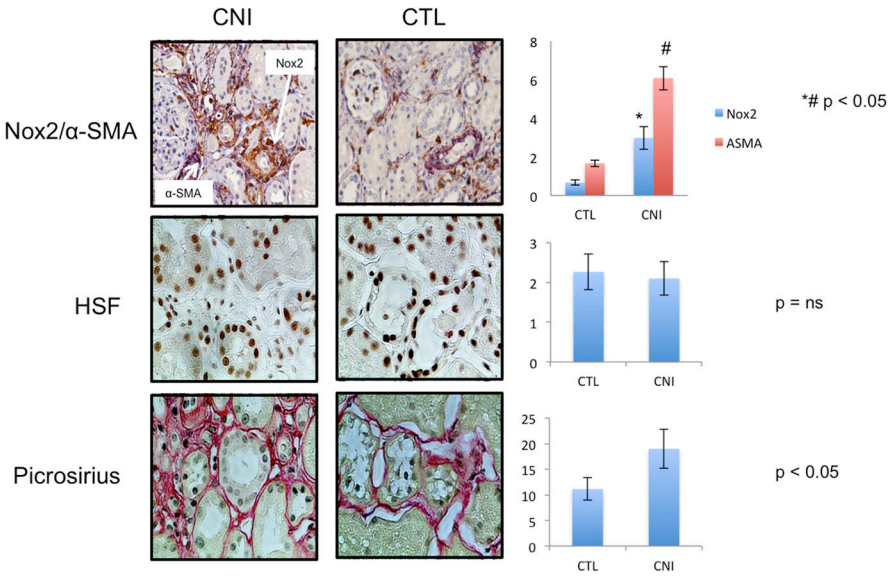


**Figure 12. Nox2 was associated with CNI induced renal fibrosis in liver transplant recipients**

Nox2 was associated with CNI induced renal fibrosis in liver transplant recipients. We determined Nox2, α-SMA, heat shock factor (HSF), and picrosirius expression in clinical biopsies from liver transplant patients diagnosed with chronic CsA nephrotoxicity compared to pre-implantation biopsies from donor kidneys (n=5 in each group). These studies revealed higher tubulointerstitial expression of Nox2 and α-SMA, and greater interstitial deposition of collagen noted by picrosirius staining.

**Table 1**

The molecular signature of chronic CsA nephrotoxicity

| Gene Symbol | Function | p-value | Fold-Change | Gene Assignment |
|---|---|---|---|---|
| Bcl9 | Injury-repair | 2.10E-03 | −1.44 | B cell CLL/lymphoma 9 |
| Capn6 | Injury-repair | 4.16E-03 | −1.69 | calpain 6 (microtubule stabilization) |
| Ctxn3 | Injury-repair | 1.93E-03 | −2.18 | cortexin 3 |
| Icam4 | Injury-repair | 3.95E-03 | −1.44 | intercellular adhesion molecule 4, Landsteiner-Wiener blood group |
| Igk | Injury-repair | 2.35E-03 | 2.36 | immunoglobulin kappa chain complex |
| Klf15 | Injury-repair | 4.15E-03 | 1.5 | Kruppel-like factor 15 |
| Neat1 | Injury-repair | 5.74E-03 | 1.71 | nuclear paraspeckle assembly transcript 1 (non-protein coding) |
| Obox1 | Injury-repair | 1.87E-03 | 1.97 | oocyte specific homeobox 1 |
| Pcdhb20 | Injury-repair | 3.34E-03 | −1.43 | protocadherin beta 20 |
| Reln | Injury-repair | 1.29E-03 | −1.4 | reelin |
| Rhox6 | Injury-repair | 2.76E-04 | −1.46 | reproductive homeobox 6 |
| Rpl39 | Injury-repair | 1.23E-03 | 1.44 | ribosomal protein L39 |
| Sfrp1 | Injury-repair | 9.18E-04 | −2.5 | secreted frizzled-related protein 1 |
| Socs2 | Injury-repair | 5.19E-04 | 1.45 | suppressor of cytokine signaling 2 |
| Spry3 | Injury-repair | 4.49E-03 | −1.57 | sprouty homolog 3 (Drosophila) |
| Traj36 | Injury-repair | 2.55E-03 | −1.71 | T cell receptor alpha joining 36 |
| Tspan13 | Injury-repair | 4.47E-03 | −1.43 | tetraspanin 13 |
| Zbtb16 | Injury-repair | 5.39E-03 | 2.75 | zinc finger and BTB domain containing 16 |
| Abcb1b | Metabolism | 3.31E-03 | 1.96 | ATP-binding cassette, sub-family B (MDR/TAP), member 1B |
| Abcc4 | Metabolism | 3.70E-03 | 1.4 | ATP-binding cassette, sub-family C (CFTR/MRP), member 4 |
| Acnat2 | Metabolism | 1.56E-03 | 2.01 | acyl-coenzyme A amino acid N-acyltransferase 2 |
| Cln8 | Metabolism | 4.24E-04 | −1.49 | ceroid-lipofuscinosis, neuronal 8 |
| Cwh43 | Metabolism | 2.01E-04 | −1.55 | cell wall biogenesis 43 C-terminal homolog (S. cerevisiae) |
| Hist1h2ac | Metabolism | 4.97E-03 | 1.44 | histone cluster 1, H2ac |
| Hmgcs2 | Metabolism | 2.79E-03 | 2.72 | 3-hydroxy-3-methylglutaryl-Coenzyme A synthase 2 |
| Nxt2 | Metabolism | 4.89E-03 | −1.44 | nuclear transport factor 2-like export factor 2 |
| Olfr1033 | Metabolism | 1.90E-03 | 1.95 | olfactory receptor 1033 |
| Olfr1054 | Metabolism | 1.05E-04 | 1.53 | olfactory receptor 1054 |

| Gene Symbol | Function | p-value | Fold-Change | Gene Assignment |
|---|---|---|---|---|
| Olfr1245 | Metabolism | 1.52E-03 | −1.51 | olfactory receptor 1245 |
| Olfr1387 | Metabolism | 9.72E-05 | −1.49 | olfactory receptor 1387 |
| Olfr1448 | Metabolism | 2.53E-03 | −1.43 | olfactory receptor 1448 |
| Pvalb | Metabolism | 4.30E-03 | −2.37 | parvalbumin |
| Vamp7 | Metabolism | 3.95E-03 | −1.63 | vesicle-associated membrane protein 7 |
| Vmn1r119 | Metabolism | 1.96E-03 | 1.45 | vomeronasal 1 receptor 119 |
| Akr1b7 | OS-Hypoxia | 5.81E-03 | 1.61 | aldo-keto reductase family 1, member B7 |
| Cyp27b1 | OS-Hypoxia | 3.95E-03 | 3.79 | cytochrome P450, family 27, subfamily b, polypeptide 1 |
| Gldc | OS-Hypoxia | 2.19E-03 | 1.82 | glycine decarboxylase |
| Hsd11b1 | OS-Hypoxia | 2.65E-03 | −2.05 | hydroxysteroid 11-beta dehydrogenase 1 |
| Maob | OS-Hypoxia | 2.95E-03 | −1.59 | monoamine oxidase B |
| Srd5a2 | OS-Hypoxia | 1.57E-03 | −2.01 | steroid 5 alpha-reductase 2 |

**Table 2**

The molecular signature of Nox2−/− in CsA nephrotoxicity

| (a) Genes from Table 1 that were significantly affected in CsA-treated wild type vs. Nox2−/− mice | | | | |
|---|---|---|---|---|
| **Gene Symbol** | **Function** | **p-value** | **Fold-Change** | **Gene Assignment** |
| Capn6 | Injury-repair | 0.01 | −1.28 | calpain 6 (involved in microtubule stabilization) |
| Igk | Injury-repair | 0.003 | −1.53 | immunoglobulin kappa chain complex |
| Neat1 | Injury-repair | 0.007 | 1.76 | nuclear paraspeckle assembly transcript 1 (non-protein coding) (cancer) |
| Obox1 | Injury-repair | 0.01 | 1.30 | oocyte specific homeobox 1 (development) |
| Abcc4 | metabolism | 0.02 | 1.22 | ATP-binding cassette, sub-family C (CFTR/MRP), member 4 |
| Cwh43 | metabolism | 0.008 | −1.25 | cell wall biogenesis 43 C-terminal homolog (S. cerevisiae) |
| Vamp7 | metabolism | 0.01 | −1.51 | vesicle-associated membrane protein 7 |
| Maob | OS-Hypoxia | 0.008 | −1.70 | monoamine oxidase B |

*Transplantation*. Author manuscript; available in PMC 2017 June 01.

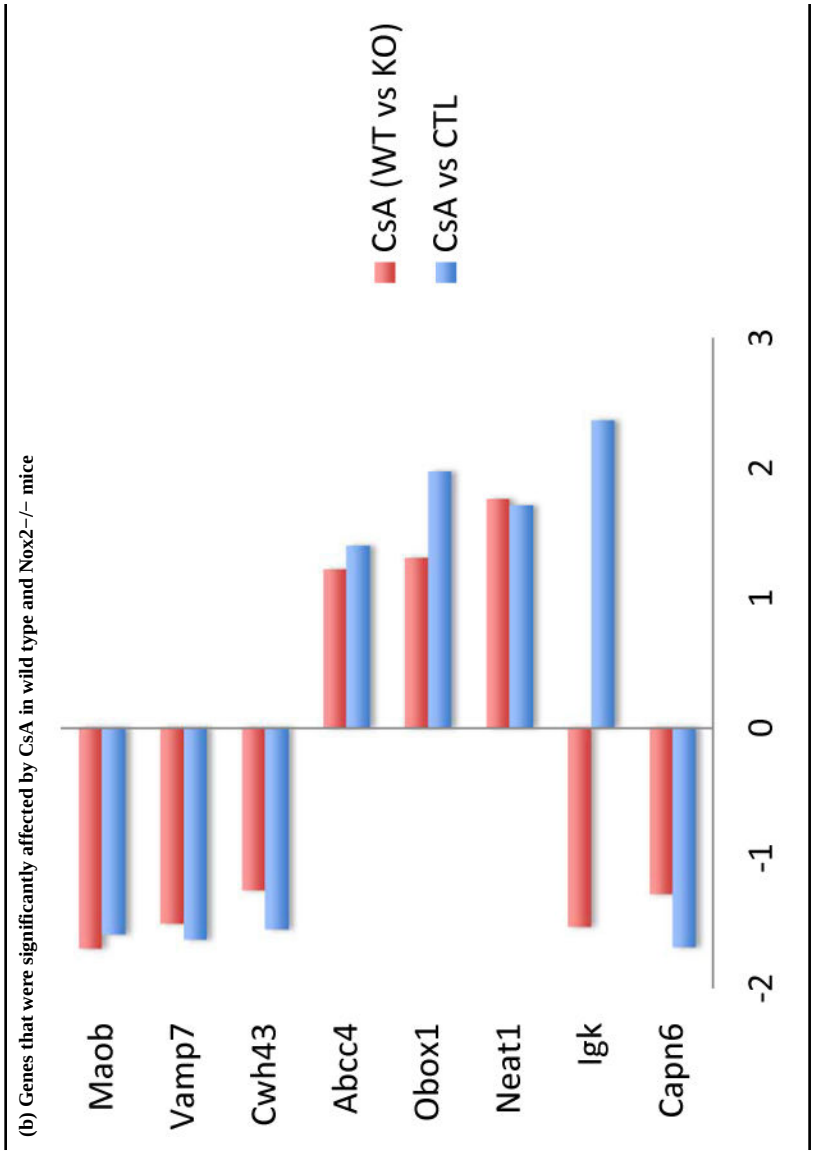


**(b) Genes that were significantly affected by CsA in wild type and Nox2−/− mice**